Sensors & Diagnostics

Accepted Manuscript

This article can be cited before page numbers have been issued, to do this please use: X. Liu, Z. Zhu, R. Sun, J. Li and S. Xu, *Sens. Diagn.*, 2025, DOI: 10.1039/D5SD00023H.

View Article Online
DOI: 10.1039/D5SD00023H

COMMUNICATION

A novel two-photon fluorescent probe for non-destructive imaging of Hg^{2+} in fresh plant tissues

Xiao Liu,[a] Zheng Zhu,[b] Ruitao Sun,[a] Jun Li*[a] and Shengzhen Xu*[a]

Received 00th January 20xx,
Accepted 00th January 20xx

DOI: 10.1039/x0xx00000x

In this work, we developed a small-molecule fluorescent probe (termed as LJTP3) for the specific detection of Hg^{2+} with an high sensitivity in living plant tissues. LJTP3 not only can effectively indicate the spatiotemporal distribution of Hg^{2+} in plant subcellular level, but also able to realize 3D imaging of Hg^{2+} in plant root.

Mercury, a highly toxic heavy metal, is widely distributed in the natural environment. However, with the increasing intensity of human activities such as industrial production, coal combustion, waste incineration and agricultural practices, mercury emissions have risen significantly, leading to serious environmental contamination [1-2]. As a major form of Hg, Hg^{2+}, exhibited a strong affinity for proteins with bioaccumulation property [3]. As a critical component of ecosystems, plants are particularly sensitive to mercury pollution [4]. Studies have shown that Hg^{2+} tends to accumulate in plant roots and leaves, and the elevated levels can cause visible damage to plant tissues and further affect plant growth and crop production [5-6]. Therefore, developing an efficient tool for the detection of Hg^{2+} in plant is great significance for agricultural management.

During the past decades, various traditional methods for detecting Hg^{2+} have been developed, including but not limited to inductively coupled plasma atomic emission spectrometry (ICP-AES), inductively coupled plasma mass spectrometry (ICP-MS), atomic fluorescence spectrometry (AFS), atomic absorption spectrometry (AAS), and chemiluminescence methods [7-10]. Compared to these techniques, fluorescent sensors displayed distinct advantages, such as high sensitivity, superior spatiotemporal resolution, and non-invasive in situ imaging capabilities [11-15]. As a result, several fluorescent probes have been employed for in vivo detection of Hg^{2+} [16-21]. However, only a few small-molecule organic fluorescent probes have been reported to achieve clear imaging at subcellular levels in plant [22-28]. Especially, two-photon fluorescent probes possess NIR excitation wavelengths, enabling deeper penetration into plant tissues to achieve plant subcellular imaging with minimum interference of background. However, some two-photon-based small-molecule probes for subcellular imaging in plants are still few, the dynamic distribution of Hg^{2+} at subcellular lever still needs to be further investigated [29-32].

In this study, a water-soluble fluorescent probe, **LJTP3** was tailored for the detection and imaging of Hg^{2+} in plant tissues. It comprises a 2-(naphthalen-2-yl)benzo[d]oxazole-based fluorophore for signal output, and a hydrophilic tetrakis (N-2-hydroxyethyl) acetamide group as Hg^{2+} specific binding component. **LJTP3** exhibited not only excellent selectivity but also a low detection limit (LOD) of 0.08 μM for early detection of Hg^{2+}. Moreover, the fluorescent signals for Hg^{2+} detection were observed in the model plant Arabidopsis, allowing visualization of its localization at the subcellular level. More importantly, the temporal and spatiotemporal distribution of mercury (Hg) was clearly observed under two-photon microscopy and 3D reconstruction.

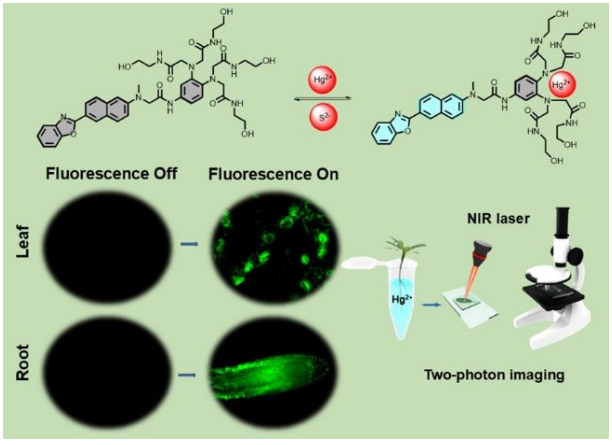

Scheme 1. Illustration of a two-photon fluorescence probe (**LJTP3**) for the detection of Hg^{2+} in Arabidopsis thaliana.

[a] College of Chemistry, Huazhong Agricultural University, Wuhan, Hubei 430070, China. E-mail: xusz@mail.hzau.edu.cn
[b] College of Life Science and Technology, Huazhong Agricultural University, Wuhan, Hubei 430070, China.
† Footnotes **X. Liu and Z. Zhu contributed equally to this work.**
Supplementary Information available: See DOI: 10.1039/x0xx00000x

View Article Online DOI: 10.1039/D5SD00037H

The synthetic procedures of **LJTP3** are shown in Scheme S1 (ESI†) and the molecular characterization data are shown in Fig. S1-S17 (ESI†). The synthesis of **LJTP3** was ultimately achieved through an 8-step process involving nucleophilic substitution, nitration, reduction, condensation reactions to get the probe with moderate yields**.**

Following the successful synthesis of **LJTP3**, evaluation of its response to Hg^{2+} was then performed in HEPES solution. As shown in Fig. S18(ESI†), the probe itself has an obvious UV absorption peak at 355 nm in HEPES solution, which was employed as excitation wavelength of **LJTP3**. The fluorescence titration experiment of **LJTP3** revealed that only Hg^{2+} induced significant fluorescence enhancement at the emission peak of 480 nm, while other metal ions including Ag^{+}, Ba^{2+}, Ca^{2+}, Cr^{3+}, Cd^{2+}, Fe^{2+}, Fe^{3+}, Mg^{2+}, Mn^{2+}, Na^{+}, Pd^{2+}, Zn^{2+} did not induce obvious fluorescence enhancement-indicating the good selectivity of **LJTP3** (Fig 1A). In addition, fluorescence interference tests for different ions were carried out in HEPES solution. As shown in Fig 1B, the fluorescence of probe **LJTP3** shows minimal interference from other coexisting metal ions, demonstrating its strong anti-interference capability. This suggests that **LJTP3** can be well-suited for the selective detection of Hg^{2+} in complex systems. The fluorescence spectra of probe **LJTP3** (1 μM) were measured at varying concentrations of Hg^{2+} (0-10 μM), as shown in Figure 1C. The fluorescence intensity gradually increased with rising Hg^{2+} concentrations, until reaching a plateau. During the titration experiments, a good linear relationship was observed between the fluorescence intensity and concentrations of Hg^{2+} in the range of 0-3 μM (Figure 1D). The limit of detection (LOD) was determined to be 0.08 μM.

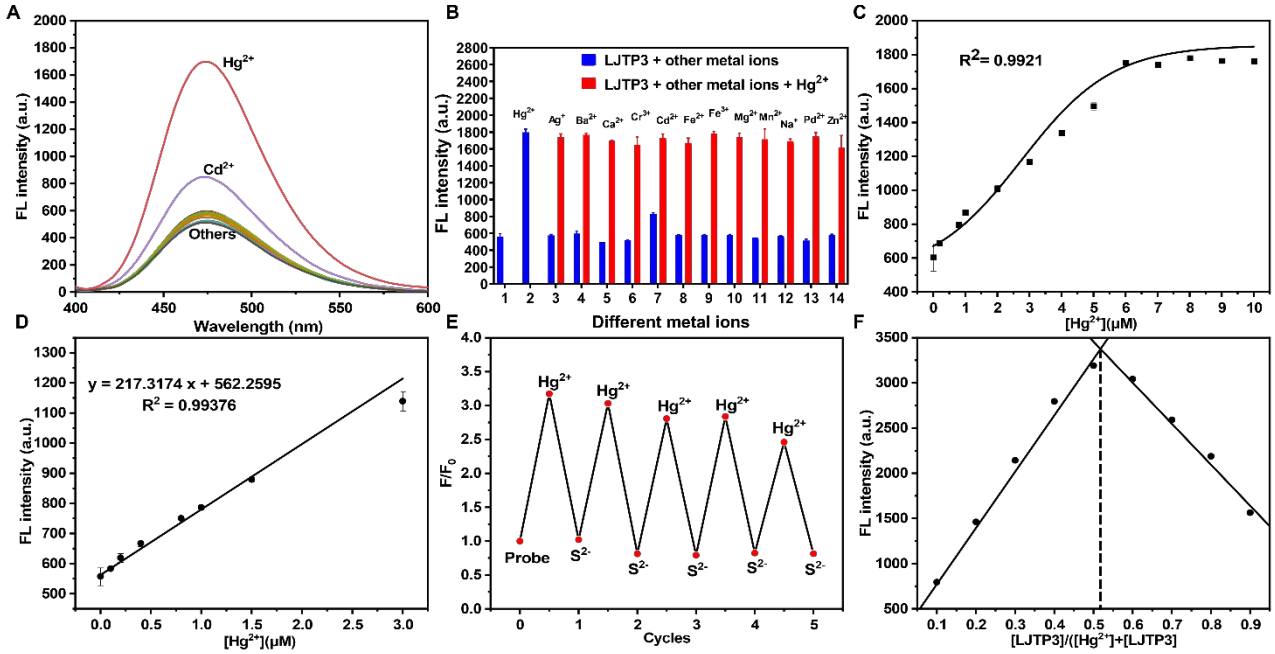

Figure 1. (A) Fluorescence response of **LJTP3** (1 μM) towards various metal ions (10 μM). including Hg^{2+}, Ag^{+}, Ba^{2+}, Ca^{2+}, Cr^{3+}, Cd^{2+}, Fe^{2+}, Fe^{3+}, Mg^{2+}, Mn^{2+}, Na^{+}, Pd^{2+}, Zn^{2+}**.** (B) Fluorescence selectivity of **LJTP3** (1 μM) with Hg^{2+} (10 μM) in the presence of various metal ions (10 μM) including 1. probe only, 2. Hg^{2+}, 3. Ag^{+}, 4. Ba^{2+}, 5. Ca^{2+}, 6. Cr^{3+}, 7. Cd^{2+}, 8. Fe^{2+}, 9. Fe^{3+}, 10. Mg^{2+}, 11. Mn^{2+}, 12. Na^{+}, 13. Pd^{2+}, 14. Zn^{2+}**.** (C) Fluorescence titration of **LJTP3** (1 μM) with different concentrations of Hg^{2+}. (D) linear relationship of **LJTP3** with difference concentrations of Hg^{2+} in the range of 0-3.0 μM. (E) Fluorescence response of LJTP3 based on emission at 480 nm in cycles of Hg^{2+} (1 μM) addition and subsequent Na_2S (1 μM) treatment. (F) Job-plots of the fluorescence intensity of **LJTP3**.

The binding mode of the probe **LJTP3** for Hg^{2+} was hypothesized, as shown in the Figure S19. Upon coordination of the polyamide ligands with Hg^{2+}, the PET effect was weakened, leading to enhanced fluorescence intensity. To confirm this hypothesis, the detection mechanism of **LJTP3** toward Hg^{2+} was thoroughly validated using ESI-MS. As shown in Fig. S20(ESI†), the molecular ion peak (M/z: 1044.3536) was observed, which matches to the calculation value (M/z: 1044.3538). Additionally, a Job-Plot experiment was conducted (Figure 1F). The intersection of the curve at a ratio of 0.5 indicates a 1:1 binding ratio between **LJTP3** and Hg^{2+}. Due to its specific affinity for S^{2-}, the Hg^{2+}-enhanced fluorescence was restored to the level of the free probe. This rapid and reversible sensing behavior was repeated five times without significant signal attenuation (Figure 1E), confirming the reversibility of the binding. Besides, **LJTP3** exhibited high stability within the pH

range of 6.5-8.0, making it suitable for Hg^{2+} sensing under physiological conditions (Fig. S21 ESI†).

To investigate the sensing mechanism (Figure 2), density functional theory (DFT) calculations were performed using Gaussian16 software [33]. The highest occupied molecular orbital (HOMO) and lowest unoccupied molecular orbital (LUMO) of **LJTP3** were primarily localized on the fluorophore, although the HOMO also exhibited partial distribution in the recognition group. The energy gap between the HOMO and LUMO was calculated to be 3.66 eV, with photo-induced electron transfer (PET) occurring from the recognition group to the fluorophore, resulting in fluorescence quenching. Upon binding with Hg^{2+}, the distribution of both the HOMO and LUMO shifted towards the fluorophore and recognition group, respectively, with a reduced energy gap of 3.45 eV, leading to the inhibition of PET and consequently, fluorescence restoration.

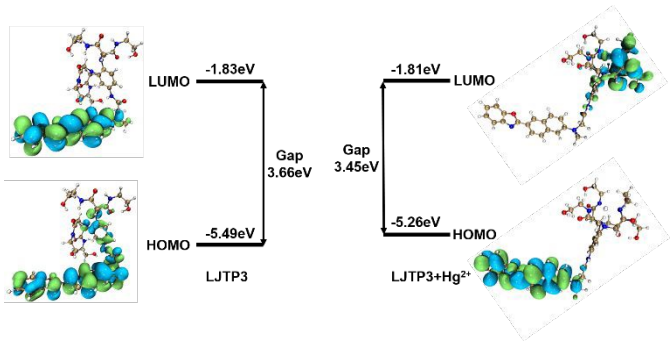

Figure 2. Molecular orbitals and corresponding energy levels of **LJTP3** and **LJTP3** + Hg^{2+} in both ground state and excitation state.

Given the advantages of two-photon microscopy, we employed this technique to further verify the probe's efficiency in detecting Hg^{2+} at the tissue and cellular level. To evaluated the probe's specificity *in vivo* test (Figure 3A-B), model plant-*Arabidopsis thaliana* was treated with various metal ions including Cd^{2+}, Mg^{2+}, Zn^{2+}, K^{+} and Hg^{2+} respectively and then imaged under two-photon microscopy (λ_{ex} = 750 nm) [34], only Hg^{2+} treated group showed significant fluorescent signal output, indicating **LJTP3** can be employed for Hg^{2+} specific imaging in plant tissues. As evidenced in Figure S23, two-photon comparative experiments were systematically conducted to examine the system before and after S^{2-} introduction. The experimental data demonstrate near-complete fluorescence quenching upon S^{2-} addition, strongly suggesting the reversible binding behavior between LJTP3 and Hg^{2+} in plant systems. In addition, the translocation of Hg^{2+} in plant tissues at subcellular level, as well as the stress response of plant cells under Hg^{2+} exposure, were visualized in a real time manner (Figure 3D-E). In the control group, where Hg^{2+} was absent, only a faint fluorescence signal was detected. However, after 1 hour of incubation with Hg^{2+}, fluorescence corresponding to the probe's interaction with Hg^{2+} appeared on the epidermal cells of the root tip. After 3 hours, the fluorescence became more widespread, reflecting a significant uptake of the probe within the root tip cells. Moreover, after 5 hours, the fluorescence intensity increased markedly, indicating a strong and clear signal. Similar trends were observed in *Arabidopsis* leaf epidermis (Figure S21C-D ESI†).

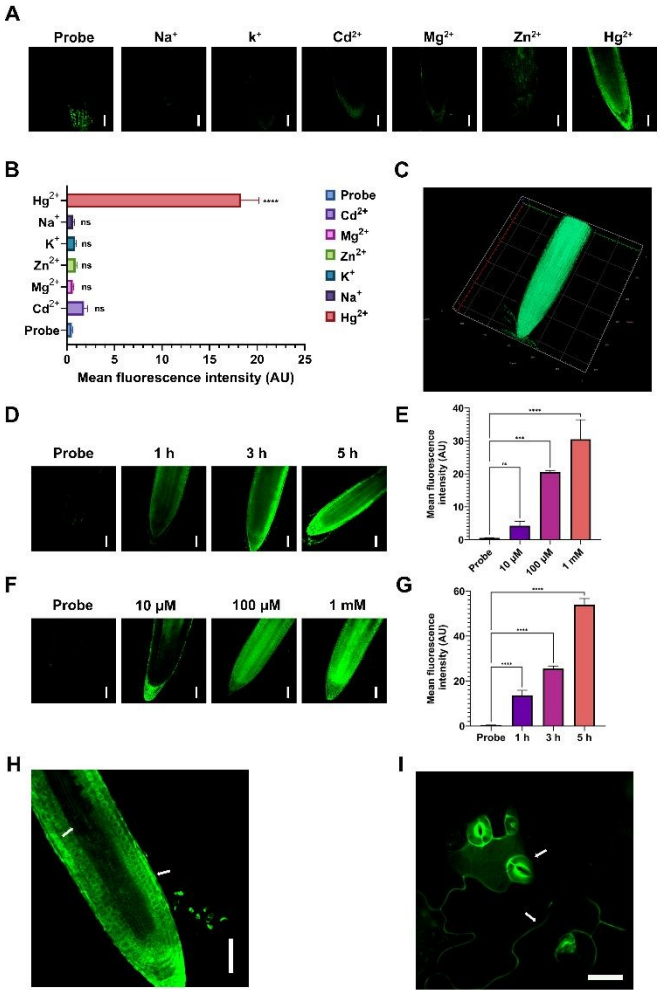

Figure 3. In Vivo Imaging of Hg^{2+} with **LJPT3**. (A-B) Elemental selective imaging fluorescence pictures of **LJPT3** and their quantitative data. (C) 3D reconstruction of **LJPT3** signal distribution in plant roots. (D-E) Fluorescence pictures of Arabidopsis root tips under different Hg^{2+} treatment times and their quantitative data. (F-G) Fluorescence pictures of Arabidopsis root tips treated with different concentrations of Hg^{2+} and their quantitative data. (H) Fine structure imaging fluorescence picture of Arabidopsis root tips. (I) Fine structure imaging fluorescence picture of Arabidopsis leaf epidermis. (scale bar = 50 μm)

To further investigate the fluorescence signal transmission in Arabidopsis under different Hg^{2+} concentrations, Two-photon imaging was performed on root tips under varying Hg^{2+} stress levels (Figure 3F-G). Only weak fluorescence signals were detected in the control group (no Hg^{2+} treatment). Under the stress of 10 μM Hg^{2+}, fluorescence signals began to appear around the cells of Arabidopsis root tips. At 100 μM Hg^{2+}, signals are present in most cells of the root tip. When the concentration was raised to 1 mM, signals appeared in all cells of the root tip

and exhibited very high fluorescence intensity. In the leaf epidermis under the same treatment, the signal changed in a similar trend (Figure S21A-B ESI†). The above results manifested that the dynamic distribution of Hg^{2+} can be visualized using LJTP3.

Under a single photon microscope with 3D imaging and reconstruction, **LJPT3** can also directly visualize the spatial distribution of Hg^{2+} in plant organs (Figure 3C). In summary, LJPT3 can realize the non-destructive detection of Hg^{2+} in plant organs and tissues in a very short time, with good selectivity and sensitivity, and can accurately indicate the location and content of Hg^{2+} in plants.

To evaluate the capability of **LJPT3** in detecting Hg^{2+} distribution differences within plant tissue microstructures, fluorescence signals in Arabidopsis root tips and leaf epidermis were analyzed using two-photon microscopy. Under 10 μM Hg^{2+} treatment, the root epidermis exhibited stronger fluorescence than the stele, reflecting a defense strategy against mercury. Likewise, the leaf epidermis showed higher fluorescence than the root stele, indicating differential Hg^{2+} accumulation (Figure 3H), consistent with previous reports.

This disparity is attributed to plant cell defense mechanisms against Hg^{2+}, aligning with previous findings [35]. In leaves, stomata exhibited stronger fluorescence than epidermal cells (Figure 3I), as they serve as key sites for Hg^{2+} exchange between plants and the environment. Plants absorb elemental mercury via stomata and convert accumulated mercury in leaves into elemental form for release [36].

In conclusion, we have designed a highly efficient fluorescent probe (**LJTP3**) specifically to study Hg^{2+} stress in plant tissues. **LJTP3** demonstrated excellent selectivity and sensitivity for early detection of Hg^{2+} in aqueous solution, with a detection limit of 0.08 μM. Remarkably, **LJTP3** exhibited outstanding selectivity for Hg^{2+} in both in vitro tests and plant imaging. Moreover, under two-photon imaging, the distribution of Hg^{2+}, along with Hg^{2+}-induced rupture of root tip cells and leaf stomata, was clearly observed. We believe this study not only provides a novel imaging tool for investigating Hg^{2+}-induced stress on plant cell structures but also contributes to the management of Hg pollution in agriculture.

Author contributions

Shengzhen Xu and Jun Li conceived the basic idea and reviewed the manuscript. Xiao Liu designed and performed the experiment and drafted the manuscript. Zheng Zhu performed the experiments and imaging; Ruitao Sun provided suggestions on experiment. All authors read and approved the manuscript. Xiao Liu and Zheng Zhu contributed equally to this work.

Conflicts of interest

There are no conflicts to declare.

Data availability

All data (experimental procedures and characterization) that support the findings of this study are available within the article and its ESI†.

Acknowledgement

This work was financially supported by Minhui Cao Studio of Huazhong Agricultural University.

Notes and references

1 C.T. Driscoll, R.P. Mason, H.M. Chan, D.J. Jacob, N. Pirrone, *Sci. Technol*, 2013, **47**, 4967–4983.
2 Y.S. Wu, A.I. Osman, M. Hosny, A.M. Elgarahy, A.S. Eltaweil, D.W. Rooney, Z.H Chen, N.S. Rahim, M. Sekar, S.C.B. Gopinath, N.N.I.M. Rani, K. Batumalaie, P.S. Yap, *ACS Omega*, 2024, **9**, 5100–5126.
3 P.A. Nogara, C.S. Oliveira, G.L. Schmitz, P.C. Piquini, M. Farina, M. Aschner, B.T. Rocha, *BBA-GEN SUBJECTS*, 2019, **1863**, 129-284.
4 B. Gworek, W. Dmuchowski, A.H. Baczewska-Dąbrowsk, *Environ. Sci. Eur*, 2020, **32**, 128.
5 J. Zhou, D. Obrist, A. Dastoor, M. Jiskra, A. Ryjkov, *Nat Rev Earth Env*, 2021, **2**, 269284.
6 W. Yuan, X. Wang, C.J. Lin, F. Wu, K. Luo, H. Zhang, Z.Y. Lu, X.B. Feng, *Environ. Sci. Technol*, 2022, **56**, 14154–14165.
7 S. Li, C.C. Zhang, S.N. Wang, Q. Liu, H.H Feng, X. Ma, J.H. Guo, *Analyst*, 2018, **143**, 4230-4246.
8 T. A. Saleh, G. Fadillah, E. Ciptawati, M. Khaled, *Trends Analyt Chem*, 2020, **132**, 116016.
9 K. Schlöglova, M. Wälle, C.A. Heinrich, *J. Anal. At. Spectrom*, 2017, **32**, 1052-1063.
10 K. Srinivasan, K. Subramanian, A. Rajasekar, K. Murugan, G. Benelli, K. Dinakaran, *Bull. Mater. Sci*, 2017, **40**, 1455-1462.
11 M.C. Dai, Y.J. Yang, S. Sarkar, K.H. Ahn, *Chem. Soc. Rev*, 2023, **52**, 6344-6358.
12 X.L. Ding, Q. Wang, D. Chen, Y.L. Chen, W.W. Pan, Q. Sun, Q. Chen, X.Y. Han, *Advanced Agrochem*, 2023, **2**, 364-370.
13 J. Yin, Y. Hu, J.Y. Yoon, *Chem. Soc. Rev*, 2015, **44**, 4619–4644.
14 Z.J. Zhang, B.R. Adhikari, P. Sen, L. Soleymani, Y.F. Li, *Advanced Agrochem*, 2023, **2**, 246-257
15 Li J., Yim D., Jang W.-D., Yoon J, *Chem. Soc. Rev*., 2017,**46**, 2437-2458.
16 L.H. Feng, Y. Deng, X.J. Wang, M.G. Liu, *Actuators B Chem*, 2017, **245**, 441-447.
17 G.J. Li, J.L. Wang, D.Y. Li, S.H. Liu, J.Yin, Z.B. Lai, G.F. Yang, *Chin. Chem. Lett*, 2021, **32**, 1527-1531.
18 J.H. Wang, Y.M. Liu, Z.M. Dong, J.B. Chao, H. Wang, Y. Wang, S.M. Shuang, *J. Hazard. Mater*, 2020, **382**, 121056.
19 L.N. Neupane, J. Park, P.K. Mehta, E.T. Oh, H.J. Park, K.H. Lee, *Chem Commun*, 2020, **56**, 2941-2944.
20 Z.G. Wang, Y. Zhang, J. Yin, Y.Q. Yang, H. Luo, J. Song, X. Xu, S.F. Wang, *Acs Sustain Chem Eng*, 2020, **33**, 12348–12359.
21 L. Wang, Y. Ma, W.Y. Lin. *J. Hazard. Mater*, 2024, **461**, 132604.
22 Y.Y. Zhang, W. Shi, D. Feng, H.M. Ma, Y. Liang, J.R. Zuo, *Sens. Actuators B Chem*, 2011, **153**, 261-265.
23 Y. Yang, R. Shen, Y.Z. Wang, F.Z. Qiu, Y. Feng, X.L. Tang, D.C. Bai, G.L. Zhang, W.S. Liu, *Sens. Actuators B Chem*, 2018, **255**, 3479-3487.
24 K. Ramki, G. Thiruppathi, S.K. Ramasamy, P. Sundararaj, P. Sakthivel, *Methods*, 2024, **221**, 1-11.
25 H.Y. Niu, T.Q. Ye, L.Y. Yao, Y.F. Lin, K. Chen, Y.B. Zeng, L. Li, L.H. Guo, J.B. Wang, *J. Hazard. Mater*, 2024, **475**, 134914.
26 Y. An, B. Li, Y.Z. Yu, Y.C. Zhou, J.F. Yi, L.P. Li, Y.Q. Sun, Z.Z. Qiang, Y.Q. Liu, P. Wang, *J. Hazard. Mater*, 2024, **465**,133331.

View Article Online
DOI: 10.1039/D5SD00023H

27 C. Zhao, A. Aziz, W.J. Lu, H.M. Xu, M. Asif, S.M. Shuang, C. Dong, *J. Hazard. Mater*, 2024, **479**, 135694.
28 J.H. Wang, Y.M. Liu, Z.M. Dong, J.B. Chao, H. Wang, Y. Wang, S.M. Shuang, *J. Hazard. Mater*, 2020, **382**, 121056.
29 J.Z. Du, K.M. Chen, Z.Y. Yu, Y.H Qiao, J.X. Liu, Q.Q. Zhai, Z. Hu, S.G. Yang, J. Li, H.L. Teng, *Advanced Agrochem*, 2022, **1**, 162-173.
30 V. Juvekar , S.J. Park , J.Y. Yoon , H.M. Kim, *Coord Chem Rev*, 2021, **427**, 213574.
31 H.W. Lee, V. Juvekar, D.J. Lee, H.M. Kim, *Trends Analyt Chem*, 2023, **165**, 117128.
32 S. Asghar, Z. Yu, Z. Zhu, D. Zheng, Z. Zhao, Y. Xu, X. Liu, C. Yuan, Y. Li, W. Wang, J.F. Xu, H.L. Teng, J. Li, W.C. Yang, C. Chen, *Research*, 2025, **8**, 0570.
33 G.J Li, J.L Wang, D.Y Li, S.H Liu, J. Yin, Z.B Lai, G.F Yan, *Chin. Chem. Lett*, 2021, **32**, 1527–1531.
34 H.J. Kim, J.H. Han, M.K. Kim, C.S. Lim, H.M. Kim, B.R. Cho. *Angew. Chem. Int. Ed*, 2010, **122**, 6938–6941.
35 J.J. Wang, Y.Y. Guo, D.L. Guo, S.L. Yin, D.L. Kong, Y.S. Liu, H. Zeng, *Environ Sci Technol*, 2012, **46**,769-777.
36 W. Yuan, X. Wang, C.J. Lin, F. Wu, K. Luo, H. Zhang, Z.Y. Lu, X.B. Feng, *Environ Sci Technol*, 2022, **56**, 14154-14165.

View Article Online
DOI: 10.1039/D5SD00023H

The authors confirm that the data supporting the findings of this study are available within the article and its supplementary materials.